
The Journal of Nuclear Medicine

JNMM

Volume 34, Number 10 • October 1993

1621 Focal Infection in HIV Patients

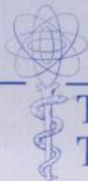
1632 Dose Planning in Benign Thyroid Diseases

1688 Reverse Redistribution in Resting Thallium Imaging

1722 Effect of Triphenyl Tetrazolium Chloride Staining

1752 A Scanning Transmission Line Source

Full Table of Contents Begins on Page 4A, Annotations on Pages 7A-8A



The Official Publication of
The Society of Nuclear Medicine, Inc.

Indium-111-Labeled Polyclonal Human Immunoglobulin: Identifying Focal Infection in Patients Positive for Human Immunodeficiency Virus

Pooled human immunoglobulin labeled with ¹¹¹In was used to identify the presence and extent of infection in 51 HIV-positive patients presenting with symptoms and/or signs of acute chest infection or with pyrexia without localizing symptoms or signs page 1621

Different Features of Pulmonary Metastases in Differentiated Thyroid Cancer: Natural History and Multivariate Statistical Analysis of Prognostic Variables

The prognostic value of age at diagnosis, sex, histologic type, tumor extension, cervical lymph node M, mediastinic M and other variables were evaluated in 134 DTC patients by univariate and multivariate analysis. page 1626

Optimal Dose Planning of Radioiodine Therapy of Benign Thyroidal Diseases

Thyroid uptake measurements were taken up to 192 hr after oral application of both 7 MBq of test activity and 150-1100 MBq of therapeutic activity in 246 patients undergoing radioiodine therapy because of benign disease. page 1632

Editorial: Optimization of Radioiodine Therapy of Thyrotoxicosis: What Have We Learned After 50 Years? page 1638

Physiopathological Significance of Thallium-201 Per Rectum Scintigraphy in Liver Cirrhosis

Direct measurement of inferior mesenteric shunting, portal pressure and cellular function, among other indices, were used to compare and evaluate the pathophysiologic significance of ²⁰¹Tl rectum scintigraphy. page 1642

Technetium-99m-Nanocolloid Scintigraphy in Orthopedic Infections: A Comparison with Indium-111-Labeled Leukocytes

Twenty-three patients with clinically suspected osteomyelitis and 21 patients with suspected prosthetic joint infection underwent both ^{99m}Tc-nanocolloid

and ¹¹¹In-labeled leukocyte scintigraphy page 1646

Clinical Immunoscintigraphy of Ovarian Carcinoma Using Iodine-131-Labeled 145-9 Monoclonal Antibody

To assess the safety, kinetics and imaging sensitivity of Mab 145-9, 2 mg of the antibody were labeled with ¹³¹I and intravenously infused in 18 patients with ovarian carcinoma page 1651

Lesion-by-Lesion Comparison of Computerized Tomography and Indium-111-Labeled Monoclonal Antibody C110 Radioimmunoscintigraphy in Colorectal Carcinoma: A Multicenter Trial

Indium-111-labeled C110 radioimmunoscintigraphy in colorectal cancer was studied in 51 pre-surgical patients at four institutions. Planar and SPECT images were obtained at least twice between 48 and 96 hr after injection. page 1656

Bispecific Monoclonal Antibody-Mediated Targeting of an Indium-111-Labeled DTPA Dimer to Primary Colorectal Tumors: Pharmacokinetics, Biodistribution, Scintigraphy and Immune Response

Eleven patients with primary colorectal carcinoma tumors were injected intravenously with 1-10 mg of a bispecific Fab'-Fab monoclonal antibody and with 1.2-4.2 nmol of ¹¹¹In-labeled DTPA dimer 2-8 days later . . page 1662

PET and the Autoradiographic Method with Continuous Inhalation of Oxygen-15-Gas: Theoretical Analysis and Comparison with Conventional Steady-State Methods

To avoid the drawbacks of the steady-state method but preserve its simplicity, a PET/autoradiographic method was applied to the build-up phase during continuous inhalation of ¹⁵O-gas, with intermittent arterial sampling. page 1672

Quantitative Analysis of PET and MRI Data in Normal Aging and

Alzheimer's Disease: Atrophy-Weighted Total Brain Metabolism and Absolute Whole Brain Metabolism as Reliable Discriminators

To validate the hypothesis that absolute glucose utilization by the brain is a more reliable indicator of Alzheimer's disease than metabolic rates calculated for a unit of brain weight, 20 patients with a probable diagnosis of AD and 17 age-matched controls underwent FDG-PET and magnetic resonance studies within a few days of each other. page 1681

Reverse Redistribution in Resting Thallium-201 Myocardial Scintigraphy in Patients with Coronary Artery Disease: Relation to Coronary Anatomy and Ventricular Function

Twenty-five patients with coronary artery disease underwent ²⁰¹Tl redistribution and resting technetium-MIBI cardiac imaging. Regional left ventricular wall motion was assessed on gated MIBI using a three-point scale page 1688

Editorial: Easy Come, Easy Go: Time to Pause and Put Thallium Reverse Distribution in Perspective page 1692

Right Ventricular Thallium-201 Kinetics in Pulmonary Hypertension: Relation to Right Ventricular Size and Function

Right ventricular size and function, and ²⁰¹Tl uptake were analyzed in 19 patients with pulmonary artery hypertension to determine if there was a relationship between thallium uptake and systolic function. page 1695

Lag Phase in Solid Gastric Emptying: Comparison of Quantification by Physiological and Mathematical Definitions

Gastric emptying studies were performed on 22 patients using a standard solid meal to calculate lag phase by three different methods: visual analysis, time-activity curves and the modified power exponential method . . . page 1701

Early Treatment Response in Malignant Lymphoma as Determined by Planar Fluorine-18-Fluorodeoxyglucose Scintigraphy

Planar ¹⁸F-FDG images obtained with a conventional gamma camera and a special collimator were compared to ⁶⁷Ga scintigraphy in 26 patients with malignant lymphoma undergoing chemotherapy page 1706

Comparison of Fluorine-18-Fluorodeoxyglucose and Carbon-11-Methionine in Head and Neck Cancer

Fourteen patients underwent a PET scan with FDG and a PET scan with ¹¹C-methionine prior to cancer therapy to compare both agents as tumor detectors. Of 21 malignant lesions, 19 were visible with both tracers. page 1711

Dopaminergic D2 Receptor SPECT Imaging in Rett Syndrome: Increase of Specific Binding in Striatum

The binding potential of ¹²³I-iodolisuride was evaluated in 11 children with Rett syndrome and 8 controls to test the hypothesis that striatal D2 receptors increase in number at the disease's early stage page 1717

Effect of Triphenyl Tetrazolium Chloride Staining on the Distribution of Radiolabeled Pharmaceuticals

The direct effect TTC has on tracer deposition was evaluated in rabbit hearts injected with teboroxime, sestamibi or ²⁰¹Tl. page 1722

Intracellular Metabolism of Indium-111-DTPA-Labeled Receptor Targeted Proteins

The in vitro and in vivo metabolism of ¹¹¹In-DTPA-labeled glycoproteins targeted to the mannose, asialoglycoprotein and mannose 6-phosphate receptors were studied in vitro using cell lines known to express these receptors and in vivo using Sprague-Dawley rats. page 1728

Bromine-76-Metabromobenzylguanidine: A PET Radiotracer for Mapping of Sympathetic Nerves of the Heart

The bromo-analog characteristics of MIBG were evaluated by biodistribution studies in rats and PET cardiac imaging in dogs to improve the quantification of the uptake of the MIBG using PET. page 1739

Scintigraphic Evaluation of Tenosynovial Giant-Cell Tumor Using Technetium-99m(V)-Dimercaptosuccinic Acid

Technetium-99m(V)-DMSA and ⁶⁷Ga-citrate scintigraphy were performed in three patients with primary and recurrent tenosynovial giant-cell tumors. page 1745

Visualization of a Recurrent Carcinoid Tumor and an Occult Distant Metastasis by Technetium-99m-Sestamibi

A carcinoid demonstrating avid uptake of sestamibi/MIBI in a recurrent bronchial carcinoid tumor and a solitary, occult bony metastatic lesion in the distal femur are presented in an atypical case page 1748

A Scanning Line Source for Simultaneous Emission and Transmission Measurements in SPECT

A microprocessor-controlled line source designed to electronically window spatial gamma camera signals to separate subject emission signals from transmission signals has been developed to simultaneously acquire emission and transmission data from a gamma camera page 1752

Optimum Sample Times for Single-Injection, Multisample Renal Clearance Methods

Times were determined by Monte Carlo simulation using a two-compartment model with parameters chosen to fit average values for ^{99m}Tc-MAG₃, ^{99m}Tc-DTPA and ¹³¹I-OIH. page 1761

Improved Formulas For The Estimation Of Renal Depth In Adults

Renal depths obtained from the Tonnesen equations were compared with those measured by computed tomography in 126 supine patients. Using stepwise linear regression analysis, a new set of equations was derived and applied to a new set of 75 patients. page 1766

Accurate Local Blood Flow Measurements with Dynamic PET: Fast Determination of Input Function Delay and Dispersion by Multilinear Minimization

The authors present a fast, multilinear least-squares minimization procedure for simultaneously determining the dispersion, blood flow and partition coefficient as a function of the delay. page 1770

Physical Performance Evaluation of the Toshiba GCA-9300A Triple-Headed System

An assessment of the physical performance of this triple-headed system and comparison, where appropriate, with another triple-headed SPECT system. page 1778

Editorial: Doing Well Under Pressure: Dedicated SPECT Cameras Come of Age. page 1789

Rapidly Converging Iterative Reconstruction Algorithms in Single-Photon Emission Computed Tomography

An iterative reconstruction method that incorporates attenuation and blur and utilizes a ramp filter to achieve results comparable to maximum-likelihood reconstruction in a fraction of the time. page 1793

Time-Dose-Fractionation in Radioimmunotherapy: Applications to Selection of Radionuclides

Differences in dose rates, biological half-lives of antibodies, physical half-lives of radionuclides and total dose required for a given biological effect were incorporated into a time-dose-fractionation approach to radioimmunotherapy. page 1801

Internal Dosimetry Using Data Derived from Autoradiographs

The nonuniformity of radiolabel distribution in tissues was studied by image analysis techniques which automatically measured the coordinates of autoradiographic grains and cell nuclei in cut sections from three different tumors following treatment with radiolabeled antibodies page 1811

Gamma Probe Assisted Detection of Small Lymph Node Metastases Following the Administration of Indium-111-Labeled Monoclonal Antibodies to Colorectal Cancers

An ex vivo probe-counting technique for the detection and staging of lymph node metastases in patients with primary colon carcinoma was validated in 13 male patients with histologically confirmed colon or rectal cancer. page 1818

Commentary: On Proselytism, Retroversion and Fiscal Nihilism in Nuclear Cardiology. page 1823